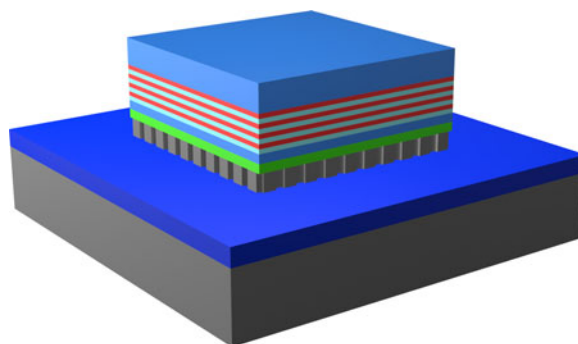


# Size Scaling of Photonic Crystal Surface Emitting Lasers on Silicon Substrates

Volume 10, Number 3, June 2018


Shih-Chia Liu  
Deyin Zhao  
Xiaochen Ge  
Carl Reuterskiöld-Hedlund  
Mattias Hammar  
Shanhui Fan, *Fellow, IEEE*  
Zhenqiang Ma, *Fellow, IEEE*  
Weidong Zhou, *Senior Member, IEEE*



---

DOI: 10.1109/JPHOT.2018.2829900  
1943-0655 © 2018 IEEE

# Size Scaling of Photonic Crystal Surface Emitting Lasers on Silicon Substrates

Shih-Chia Liu,<sup>1</sup> Deyin Zhao,<sup>1</sup> Xiaochen Ge,<sup>1</sup>  
Carl Reuterskiöld-Hedlund,<sup>2</sup> Mattias Hammar,<sup>2</sup>  
Shanhui Fan,<sup>3</sup> *Fellow, IEEE*, Zhenqiang Ma,<sup>4</sup> *Fellow, IEEE*,  
and Weidong Zhou ,<sup>1</sup> *Senior Member, IEEE*

<sup>1</sup>Department of Electrical Engineering, University of Texas at Arlington, Arlington, TX 76019 USA

<sup>2</sup>KTH-Royal Institute of Technology, School of Information and Communication Technology, Kista 164 40, Sweden

<sup>3</sup>Department of Electrical Engineering, Stanford University, Stanford, CA 94305 USA

<sup>4</sup>Department of Electrical and Computer Engineering, University of Wisconsin-Madison, Madison, WI 53706 USA

DOI:10.1109/JPHOT.2018.2829900

1943-0655 © 2018 IEEE. Translations and content mining are permitted for academic research only. Personal use is also permitted, but republication/redistribution requires IEEE permission. See [http://www.ieee.org/publications\\_standards/publications/rights/index.html](http://www.ieee.org/publications_standards/publications/rights/index.html) for more information.

Manuscript received March 27, 2018; revised April 17, 2018; accepted April 19, 2018. Date of publication April 27, 2018; date of current version May 16, 2018. This work was supported in part by the U.S. National Science Foundation and in part by ARO under Grant W911NF-15-1-0431 (PM: Dr. M. Gerhold). The work of M. Hammar was supported by the Swedish Research Council (VR). Corresponding author: Weidong Zhou (email: wzhou@uta.edu).

**Abstract:** We report here the lateral cavity size scaling and confinement effects on the lasing performance in defect-free photonic crystal surface-emitting lasers (PCSEL) on silicon substrates. Hybrid PCSELS with different lateral cavity sizes and different lateral confinement geometries have been fabricated using transfer printing technology and controlled selective etching. The measured lasing properties show a strong dependence on the lateral cavity size below 100  $\mu\text{m}$ . In particular, the finite lateral dimension significantly affects the laser threshold and side mode suppression ratio (SMSR) of the PCSEL devices. On the other hand, by controlling the lateral confinement using vertical etching, a reduction of the laser threshold is observed. The experimental results agree well with theoretical predictions. The work presented here can lead to ultra-compact PCSELS for on-chip integration with excellent energy efficiency.

**Index Terms:** Photonic crystals, silicon photonics, lasers, heterogeneous.

## 1. Introduction

The realization of CMOS compatible lasers on silicon (Si) remains an active and challenging area of research for integrated Si photonics [1]. The heterogeneous integration of III-V semiconductor active layers with the Si substrate seems to be one of the most promising approaches. Various III-V/Si hybrid lasers have been reported, either by bonding or printing III-V gain materials to Si [2]–[5] or the growth of III-V materials directly on Si [6]–[8]. Recently, large area defect-free photonic crystal surface-emitting lasers (PCSELS) fabricated using transfer-printing on both SOI and bulk Si substrates were reported [9], [10]. Based on the bandedge effect in the photonic crystal (PC) structure, strong in-plane coupling occurs due to multidirectional Bragg diffraction [11], and the formation of a two-dimensional (2D) PC cavity mode with surface-normal emission. Recent

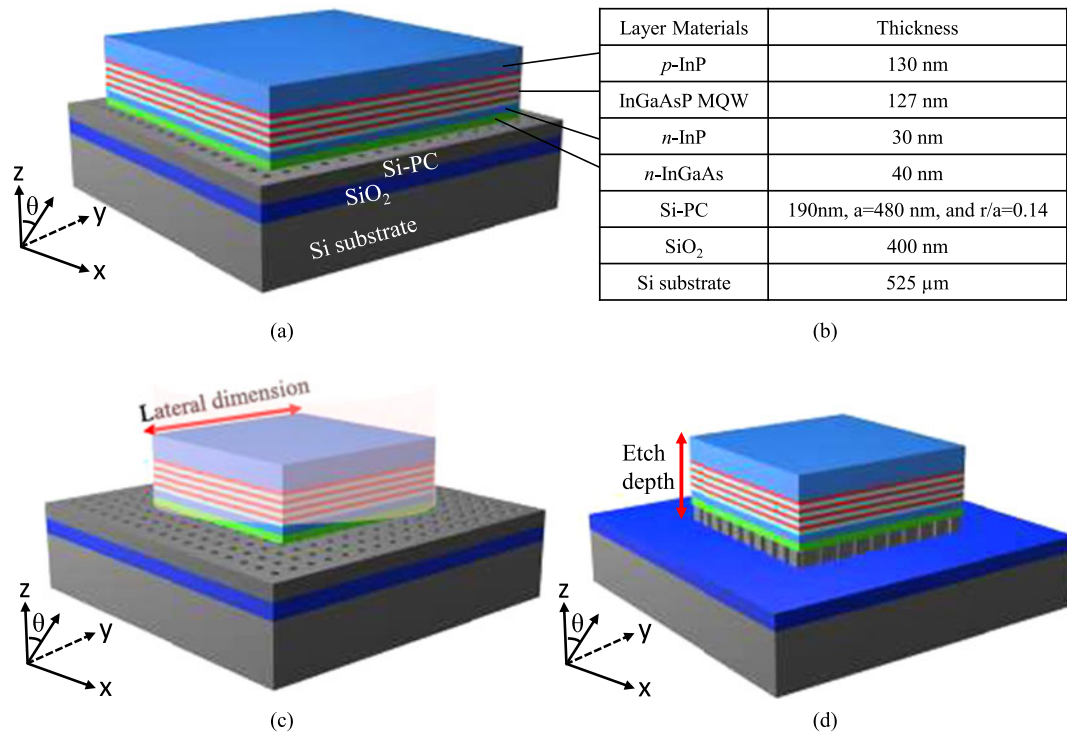


Fig. 1. (a) Schematic of PCSEL with  $600 \times 600 \mu\text{m}^2$  size. (b) Cavity design. (c) Schematic of PCSEL with variation in lateral dimension (L). (d) Schematic of PCSEL with variation in vertical etch depth.

progress in the development of PCSELs has demonstrated various advantages such as large-area singlemode emission, narrow linewidth, high output power, and small divergence angle [12]–[17]. In fact, a large lateral cavity size is necessary to obtain low threshold lasing conditions due to the negligible in-plane cavity losses [12].

However, the scaling of on-chip lasers demand compact cavity sizes in order to achieve high energy efficiency and high speed operation. The reduction in lateral cavity size for PCSELs may result in a reduced in-plane confinement (quality factor) and thus increased lasing threshold [18]. Here we report a detailed theoretical and experimental investigation on the lateral cavity size scaling and lateral cavity confinement and their effects on optical cavity quality factor ( $Q$ ), confinement factor ( $\Gamma_{QW}$ ) and gain threshold ( $g_{th}$ ) as well as the resulting laser modal and spectral properties, including the emission wavelength and side-mode suppression ratio (SMSR).

## 2. Device Design

Fig. 1(a) shows a schematic illustration of a PCSEL on a SOI substrate, where a  $600 \times 600 \mu\text{m}^2$  InGaAsP multi-quantum-well (MQW) heterostructure membrane layer has been transferred and printed onto a Si PC cavity. The InP based layer structure and Si PC parameters are indicated in Fig. 1(b). The 2D square-lattice Si PC structure is designed to have a lattice constant ( $a$ ) of 480 nm, based on second-order Bragg condition for an emission wavelength around 1,540 nm [12], [15]. Single mode lasing under room-temperature (RT) operation was observed with a narrow linewidth of 0.54 nm and excellent SMSR of 31.8 dB [9], [10].

To investigate the lateral confinement effect, we considered two control parameters. First, we adjust the lateral cavity size by controlling the pumping beam spot size, as shown in Fig. 1(c). We also experimentally fabricated various laser cavity sizes to define the lateral dimensions. Secondly, for a fixed lateral cavity size, we adjust the lateral confinement by controlling the etch depth defining

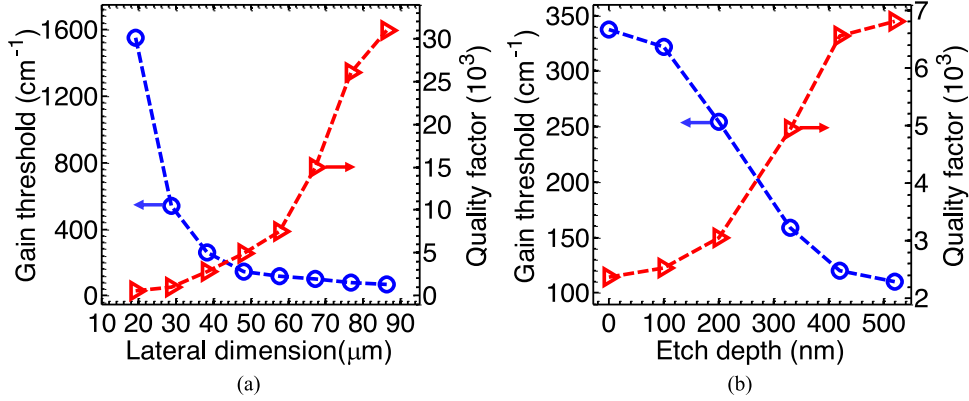


Fig. 2. (a) The simulated gain thresholds and  $Q$  factors for different device lateral dimensions; and (b) The simulated gain thresholds and  $Q$  factors for a device with lateral dimension of  $48\ \mu\text{m}$  ( $L = 100a$ ) at different etching depths.

the cavity region as shown in Fig. 1(d). Theoretical investigations were first carried out to estimate the cavity  $Q$  factor and the associated gain thresholds for different lateral and vertical dimensions. The simulations of reflection spectra were carried out using the Fourier Modal Method with Stanford Stratified Structure Solver ( $S_4$ ) software package. The  $Q$  factor was calculated by fitting the guided Fano resonance peaks or dips in the simulated reflection spectra [19]. In addition, the field distribution is computed with a finite-difference time-domain (FDTD) based software MEEP [20], and the confinement factor can be calculated as follows [10]:

$$\Gamma_{QW} = \frac{\int_{QW} E^2 \cdot dv}{\int_{cav} E^2 \cdot dv} \quad (1)$$

Therefore, the corresponding threshold gain was estimated according to [10], [12]:

$$g_{th} = \frac{\alpha}{\Gamma_{QW}} = \frac{2\pi}{Q \cdot a} \times \frac{1}{\Gamma_{QW}} \quad (2)$$

where  $a$  is the lattice constant and  $\alpha$  is the loss in the laser cavity. In our calculations, only the in-plane loss and vertical radiation loss are considered, and the internal loss is negligible [12].

Shown in Fig. 2(a) are the calculated threshold gains and  $Q$  factors for different lateral cavity sizes. The  $Q$  factor drops rapidly while the threshold gain increases with decreasing device size from  $80\ \mu\text{m}$  to  $20\ \mu\text{m}$ . This indicates that the influence of in-plane loss has to be taken into account for finite device sizes. In other words, the limited extension of the Si PC reduces the in-plane coupling efficiency. As a result, power escapes from the edges of the laser cavity due to weak lateral confinement.

To reduce the cavity loss due to the finite lateral dimensions, some lateral confinement can be introduced. Here we investigate a simple lateral confinement scheme by controlling the etch depth of the lasing cavity (lateral index contrast). The result is shown in Fig. 2(b) for a PCSEL on Si with a lateral cavity dimension of  $48\ \mu\text{m}$  ( $L = 100a$ ). By increasing the etch depth from 0 to 500 nm, which corresponds to the complete removal of the InGaAsP QW heterostructure and Si PC cavity (Fig. 1(d)), the cavity  $Q$  factor increases from 2,300 to 6,800. We attribute this to the increased lateral confinement due to the increased lateral index contrast.

### 3. Experimental Results

To verify these effects experimentally, we investigated a PCSEL on Si substrate with transferred InGaAsP membrane lateral dimension of  $600 \times 600\ \mu\text{m}^2$  [9], [10]. The finite-size effect was first investigated to understand the importance of laser output characterizations related to the optical pumping spot size [21]. Here the lateral cavity dimension was defined by the excitation area of

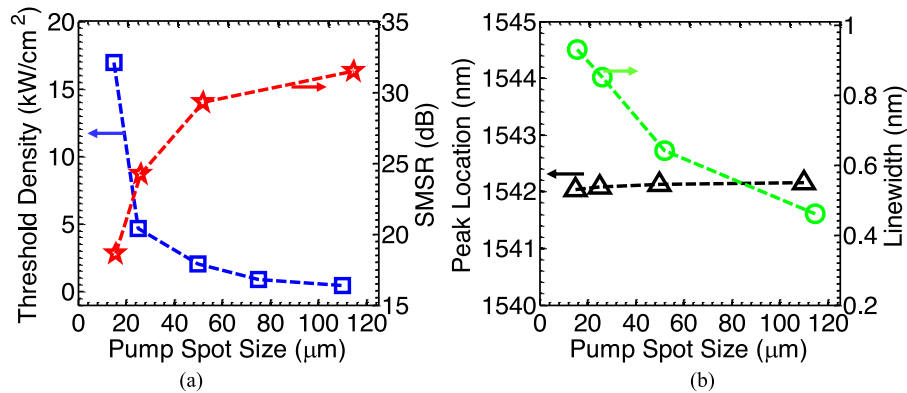


Fig. 3. (a) The lasing threshold and SMSR as a function of the pump spot size. (b) Lasing peak wavelength locations and corresponding linewidths as a function of the pump spot size.

the beam spot. A continuous wave (c.w.) green (532 nm) laser was used as the pump source incident from the surface normal direction via a long working distance objective lens (x10). The diameter of the excitation spot was around 110 μm. Another long working distance objective lens (x50) was added to the measurement system along with precision pinholes to further reduce the spot size to 50 μm, 25 μm, and 15 μm, respectively. It should be noted that the pump energy is normalized to the excitation area for comparison. The measured results are shown in Fig. 3. The measured lasing threshold density increases from 0.42 kW/cm<sup>2</sup> to around 16.8 kW/cm<sup>2</sup> when the pump spot size reduced from 110 to 15 μm, while the SMSR decreased from 31.4 to 18.6 dB. The lasing linewidth also increased when the pump spot size reduces to 50 μm or less (Fig. 3 (b)). These results indicate that for a reduced spot size, the device is excited at a state of weak lateral confinement with low coupling efficiency. Due to the reduced coupling strength, the laser threshold is much higher compared to the case a larger spot size. Conversely, when the pump spot size is increased to beyond 100 μm, the device is excited at a state of strong lateral confinement with high coupling efficiency and threshold density cannot be further decreased but reaches a saturation value. On the other hand, the emission wavelength peak slightly blue-shifted as the pumping spot size decreased, which indicates the lateral cavity size also slightly impacts the cavity effective index.

Next, we experimentally demonstrated the lateral confinement effect by fabricating various PCSELs with different cavity sizes and etch depths (Fig. 4). The relatively large MQW membrane (600 μm) was considered as defining the zero vertical etch depth (Fig. 4(a)), where the cavity dimension was defined solely by the excitation area. Secondly, various devices of relatively small PCSELs including 30 μm, 50 μm, 75 μm, and 100 μm dimensions were patterned using standard photolithography and controlled etching. The first investigated etch depth was 330 nm, where only the top InGaAsP MQW membrane was etched away as shown in Fig. 4(b). The devices were characterized at this point and thereafter further etched down to 520 nm, so that the top QW layer and bottom Si PC layer were completely removed, thereby exposing the BOX layer as shown in Fig. 4(c).

The measured lasing threshold density versus device size is shown in Fig. 4(d). We note that the lasing threshold density increases with decreasing device size for the three cavity geometries. Additionally, the threshold power density shows an inverse relationship with the vertical etch depth. The SMSR, in contrast, shows quite a different behavior as shown in Fig. 4(e). The SMSR decreases with decreasing device size. This behavior can be understood as follows. For a small device size, the major loss mechanism in the laser is the in-plane loss. In particular, for a very short cavity dimension, the high threshold density is mainly due to the energy leakage through the gain region at the boundary of the laser cavity. For a relatively smaller device sizes ( $L < 70$  μm) the influence of in-plane loss on the threshold power is drastically increased which leads to significantly higher threshold power density and lower SMSR in the lasing characteristics. However, in the case of

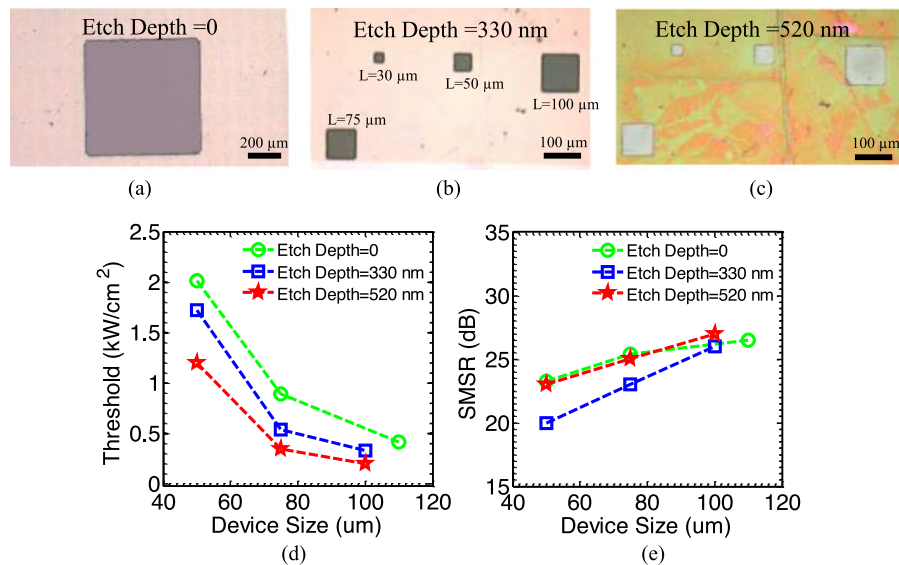


Fig. 4. (a) Optical microscope image of  $600 \times 600 \mu\text{m}^2$  PCSEL on Si PC cavity. (b) Image of PCSELs with different size at 330 nm vertical etching depth. (c) Image of PCSELs with different size at 520 nm vertical etching depth. (d) Measured lasing threshold power density of three cavity configurations versus device size. (e) Measured SMSR for the three cavity configurations versus device size.

deeper vertical etch depth, the large refractive index contrast between the Si PC and air at the cavity boundary provides sufficient coupling feedback and enhanced lateral confinement.

#### 4. Conclusion

In conclusion, we have demonstrated RT operation of PCSELs on Si substrate based on transfer printing technology and analyzed them both theoretically and experimentally. Various devices with different cavity dimensions were fabricated to investigate the lasing characteristics. For small device dimensions, the threshold increases due to increased in-plane loss and to reduce the threshold and to maintain lasing oscillation also in these cases, a strong lateral confinement is necessary. This was successfully realized using a selective etching process for increased effective index contrast. In combination with our previous findings that the design of the adjacent grating and bottom metal reflector also can be effective in mitigating the in-plane loss at the device boundary [22], this demonstrates a good potential for ultra-compact and power-efficient PCSEL devices.

#### Acknowledgment

Dr. Zhou has a potential research conflict of interest due to a financial interest with company Semerane. A management plan has been created to preserve objectivity in research in accordance with UTA policy.

#### References

- [1] Z. Wang, "Novel light source integration approaches for silicon photonics," *Laser Photon Rev.*, vol. 11, 2017, Art. no. 1700063.
- [2] H. Park, A. W. Fang, O. Cohen, R. Jones, M. J. Paniccia, and J. E. Bowers, "Design and fabrication of optically pumped hybrid silicon-AlGaInAs evanescent lasers," *IEEE J. Sel. Topics Quantum Electron.*, vol. 12, no. 6, pp. 1657–1663, Nov./Dec. 2006.
- [3] J. Van Campenhout *et al.*, "Electrically pumped InP-based microdisk lasers integrated with a nanophotonic silicon-on-insulator waveguide circuit," *Opt. Exp.*, vol. 15, pp. 6744–6749, May 2007.
- [4] H. Yang *et al.*, "Transfer-printed stacked nanomembrane lasers on silicon," *Nature Photon.*, vol. 6, pp. 615–620, 2012.



- [5] J. Justice, C. Bower, M. Meitl, M. B. Mooney, M. A. Gubbins, and B. Corbett, "Wafer-scale integration of group III–V lasers on silicon using transfer printing of epitaxial layers," *Nature Photon.*, vol. 6, pp. 610–614, 2012.
- [6] R. Chen *et al.*, "Nanolasers grown on silicon," *Nature Photon.*, vol. 5, pp. 170–175, 2011.
- [7] Z. Mi, P. Bhattacharya, J. Yang, and K. P. Pipe, "Room-temperature self-organised  $\text{In}_{0.5}\text{Ga}_{0.5}\text{As}$  quantum dot laser on silicon," *Electron. Lett.*, vol. 41, pp. 742–744, 2005.
- [8] S. Chen *et al.*, "Electrically pumped continuous-wave III–V quantum dot lasers on silicon," *Nature Photon.*, vol. 10, pp. 307–311, 2016.
- [9] D. Zhao *et al.*, "Printed large-area single-mode photonic crystal bandedge surface-emitting lasers on silicon," *Sci. Rep.*, vol. 6, 2016, Art. no. 18860.
- [10] S.-C. Liu *et al.*, "Photonic crystal bandedge membrane lasers on silicon," *Appl. Opt.*, vol. 56, pp. H67–H73, 2017.
- [11] M. Imada, A. Chutinan, S. Noda, and M. Mochizuki, "Multidirectionally distributed feedback photonic crystal lasers," *Phys. Rev. B*, vol. 65, Apr. 26, 2002, Art. no. 195306.
- [12] K. Hirose, Y. Liang, Y. Kurosaka, A. Watanabe, T. Sugiyama, and S. Noda, "Watt-class high-power, high-beam-quality photonic-crystal lasers," *Nature Photon.*, vol. 8, pp. 406–411, 2014.
- [13] M. Imada, S. Noda, A. Chutinan, T. Tokuda, M. Murata, and G. Sasaki, "Coherent two-dimensional lasing action in surface-emitting laser with triangular-lattice photonic crystal structure," *Appl. Phys. Lett.*, vol. 75, pp. 316–318, Sep. 19, 1999.
- [14] S.-L. Chua, L. Lu, J. Bravo-Abad, J. D. Joannopoulos, and M. Soljačić, "Larger-area single-mode photonic crystal surface-emitting lasers enabled by an accidental Dirac point," *Opt. Lett.*, vol. 39, pp. 2072–2075, Apr. 1, 2014.
- [15] M. Meier *et al.*, "Laser action from two-dimensional distributed feedback in photonic crystals," *Appl. Phys. Lett.*, vol. 74, pp. 7–9, 1999.
- [16] S. Noda, M. Yokoyama, M. Imada, A. Chutinan, and M. Mochizuki, "Polarization mode control of two-dimensional photonic crystal laser by unit cell structure design," *Science*, vol. 293, pp. 1123–1125, 2001.
- [17] L. Javier Martínez *et al.*, "Two-dimensional surface emitting photonic crystal laser with hybrid triangular-graphite structure," *Opt. Exp.*, vol. 17, pp. 15043–15051, Aug. 17, 2009.
- [18] Y. Liang, C. Peng, K. Sakai, S. Iwahashi, and S. Noda, "Three-dimensional coupled-wave analysis for square-lattice photonic crystal surface emitting lasers with transverse-electric polarization: Finite-size effects," *Opt. Exp.*, vol. 20, pp. 15945–15961, Jul. 2, 2012.
- [19] A. E. Miroshnichenko, S. Flach, and Y. S. Kivshar, "Fano resonances in nanoscale structures," *Rev. Modern Phys.*, vol. 82, pp. 2257–2298, Nov. 8, 2010.
- [20] A. F. Oskooi, D. Roundy, M. Ibanescu, P. Bermel, J. D. Joannopoulos, and S. G. Johnson, "Meep: A flexible free-software package for electromagnetic simulations by the FDTD method," *Comput. Phys. Commun.*, vol. 181, pp. 687–702, 2010.
- [21] X. Liu *et al.*, "Pump spot size dependent lasing threshold in organic semiconductor DFB lasers fabricated via nanograting transfer," *Opt. Exp.*, vol. 21, pp. 27697–27706, 2013.
- [22] D. Zhao *et al.*, "Lateral size scaling of photonic crystal bandedge lasers on SOI substrates," *The 12th Int. Symp. Photon. Electromagn. Crystal Struct. (PECS-XII)*, University of York, UK, Jul. 17–21, 2016.